Scalable Synthesis of Selective Hydrodeoxygenation Inverted Pd@TiO_2 Nanocatalysts

Authors: Pinaki Ranadive,[1] Zachary Blanchette,[2] Alex Spanos,[1] J. Will Medlin,[2] and **Nicholas Brunelli***[,1]

Author address: [1] The Ohio State University, William G. Lowrie Department of Chemical and Biomolecular Engineering, 151 W. Woodruff Ave., Columbus, OH 43210; [2] University of Colorado, Department of Chemical and Biological Engineering, Boulder, CO 80303

***Corresponding author:** brunelli.2@osu.edu; Twitter: OSUChemEProfBru

Abstract

Novel developments in catalytic nanomaterials will enable more sustainable processes provided that scalable synthetic methods can be developed. Recently, inverted systems consisting of palladium nanoparticles (Pd NPs) encapsulated in a porous titania shell (Pd@TiO_2) that has micropores have been associated with high selectivity for hydrodeoxygenation. These catalysts are currently synthesized in low-throughput batch processes that can be difficult to scale because of poor mixing at large scales. Mixing can be controlled through a continuous jet-mixing reactor that has been previously demonstrated to produce monodisperse nanomaterials. A jet-mixing process is developed for continuous Pd@TiO_2 synthesis by evaluating the effect of important synthesis parameters in batch. Pd@TiO_2 synthesized through jet-mixing is found to contain comparable microporosity to its lab scale batch-synthesized counterpart. The materials produced using the jet-mixing reactor achieve >99.3% selectivity for the HDO product (i.e., toluene) over the decarbonylation product (benzene). Overall, these results demonstrate that the continuous jet-

mixing reactor is a promising technology for scalable production of selective Pd@TiO_2 nanocatalysts.

Article highlights:

- Continuous scalable jet-mixing process developed for controlled environment Pd@TiO_2 nanomaterial synthesis
- Integration of a controlled environment sample collection system enables use of water sensitive reagents.
- Flow-synthesized Pd@TiO_2 achieves high selectivity (>99.3%) towards benzyl alcohol HDO

Keywords: Continuous synthesis; catalytic nanomaterials; process development; HDO; inverted catalyst

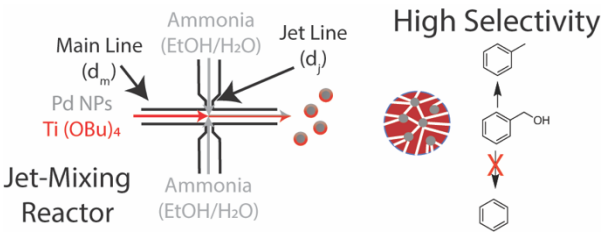

1. Introduction

Advancements in the synthesis of nanomaterial catalysts have impacted many fields, including the conversion of biomass to value-added fuels and chemicals [1,2]. Indeed, the development of novel catalyst configurations and morphologies has produced materials with improved selectivity towards desired products [3–9]. A key challenge that hinders commercial application of these exciting results is the translation of the lab-scale syntheses of these materials

to bulk production. Currently, these syntheses are performed in small-volume batch reactors. Batch synthesis methods are hindered by low process throughput and process variability that results in materials with a distribution of properties, including a broad nanoparticle size distribution. These challenges can be attributed to differences in mixing as the process is scaled-up, which typically results in poor mixing [10]. Hence, there is a need for the development of processes that synthesize supported catalysts in a scalable manner while retaining the quality obtained at the lab scale.

An attractive model system is to use inverted nanomaterial catalysts. Inverted nanomaterial catalysts are comprised of metal nanoparticles encapsulated within a porous metal oxide film, forming a composite material [3,4,11]. These materials have better catalytic activity [2,12–17] and stability [6,18] than traditional supported catalysts. Inverted systems can be synthesized using different methods, including (1) oxide deposition, (2) single-step syntheses, and (3) two-step syntheses [8]. Oxide deposition methods involve deposition of metal nanoparticles on a metal oxide, that is further coated with metal oxide using chemical deposition techniques such as atomic layer deposition [5]. Although the atomic-scale control over film thickness makes synthesis reproducible, high temperature treatment post synthesis is necessary to induce porosity in the shell and restore catalytic activity [6]. This can cause undesired alterations in the catalytic structure. A single-step synthesis method combines both the metal and metal-oxide components are synthesized simultaneously from the bottom-up [19,20]. Whereas this technique is attractive because of the low cost associated with a single step and the potential ease of scale-up, it is challenging to achieve precisely controlled shape, size, and morphology of the inverted structures [21,22]. Two-step methods involve the synthesis of unsupported metal nanoparticles before oxide overlayer deposition. This is an alternative approach that improves the controllability of the synthesis since the metal NPs can be pre-synthesized and used as “seeds” in the synthesis of the

metal oxide shell. A common technique in two-step syntheses is growth of the metal oxide on functionalized metal NPs [21]. Functionalized growth incorporates ligands or surfactants with specific binding groups on the metal NPs post-synthesis that reduce the interfacial energy between the metal and metal oxide and make synthesis energetically favorable [4,23]. Further, porosity in oxide shells can be introduced using surfactant micelle arrays without additional heat treatment, making this a favorable technique [24,25].

Two-step synthesis has recently been used for the synthesis of inverted Pd@TiO_2 nanocatalysts [17]. These materials have demonstrated improved selectivity for the hydrodeoxygenation (HDO) of aromatics, an important step in biomass conversion that is used as a test reaction. The improvement in selectivity is attributed to the high microporosity in the Pd@TiO_2 catalyst. Specifically, increasing the microporosity in the titania shell is correlated to the blocking of a secondary, undesirable decarbonylation pathway [11,17]. Interestingly, the microporosity of the material was controlled by the rate of hydrolysis of the titanium precursor during synthesis, benefitting from rapid mixing that can be achieved at small scale. These studies are promising provided that they can be scaled up. Currently, they are conducted at a small scale in batch reactors that produce limited throughput per batch [11,17].

On increasing size, batch reactors may also suffer from batch-to-batch variability that is caused by slight differences in parameters such as injection rate of reactants, variation in stirring speed and geometry, and the method of heating [26,27]. Indeed, the mixing time for lab scale reactors is estimated to be on the order of seconds[28] whereas large reactor can have mixing times up to 200 s [29]. This is especially significant for fast processes in which the reaction time is much smaller than the time taken to achieve concentration homogeneity in solution. Precursors of oxides such as titania are highly reactive and undergo fast hydrolysis to form the porous oxide network,

affecting its properties [30]. This necessitates a synthesis technique that can provide high controllability over the hydrolysis step, in addition to being scalable.

A promising alternative to batch synthesis is continuous flow synthesis. Flow processes offer improved heat and mass transfer rates owing to their high internal surface area and high control over the rate and time of addition of reagents [28,31]. This reduces the variability associated with products synthesized via flow processes [32]. Millifluidic or microfluidic flow reactors have a compact volume that reduces the extent of mixing required to achieve homogeneity [33]. The small volume results in a mixing time that is an order of magnitude smaller than batch processes, making it possible to achieve spatially uniform nanoparticle nucleation and growth. For fast processes such as hydrolysis, this leads to uniformity in particle properties [33,34]. Flow processes also benefit from ease of automation and integration of process control in the system as compared to a batch process. Most importantly, flow syntheses can be readily scaled-up by increasing reactor run-time or scaling out the number of reactors operating in parallel [35]. Indeed, flow reactors used for nanoparticles synthesis have shown improved product properties as compared to batch processes [10,36].

Several geometries have been used in designing microreactors. Three widely used ones are coaxial jets [37–40], impinging jets [23,34,41–43], and segmented flow [44–47]. In coaxial jet reactors, one of the reactant streams is directed axially into a wider tube containing the second reactant. This orientation can result in efficient mixing provided radial mixing can be maximized. [37,39] Impinging jet reactors consist of the two reactant streams mixing at an angle and are easy to fabricate. However, the mixing zone can be large and may result in a spread in particle properties [38]. The segmented flow reactor is known to achieve monodisperse size distributions because of minimized axial dispersion provided gas and liquid velocities are controlled [48].

Efficient mixing and design simplicity are key to a scalable process. Recently, our group has developed a jet-mixing reactor, based on a previous gas-phase synthesis, that can promote mixing because of narrow jets perpendicularly impinging a main line [49]. The estimated mixing time has been calculated as 22 ms at conditions that commonly used in this work (see supplemental information for more details). The simple reactor design enables easy fabrication and offers flexibility in applications. We have demonstrated the successful continuous synthesis of zeolitic imidazolate framework (ZIF-8) and silver nanoparticles (Ag NPs) using the jet-mixing reactor [32,50]. The reactor led to higher reproducibility, narrower size distribution, and increased shelf life for Ag NPs as compared to conventional batch synthesis.

Additionally, the modularity of the jet-mixing reactor is ideal for sequential processes such as Pd@TiO_2 synthesis where reagents need to be introduced controllably in multiple steps at specified residence times. Specifically, two jet-mixing reactors can be readily assembled in series - the first for the synthesis of Pd NPs and the second for Ti-precursor hydrolysis to coat the Pd NPs with TiO_2. Preliminary work in designing this process involves successful design of a single-step process that coats pre-formed Pd NPs with titania.

Currently, Pd@TiO_2 inverted nanomaterials have not been produced using a flow process. In this work, we will focus on synthesis of the porous titania shell of the Pd@TiO_2 in a continuous manner using the jet-mixing reactor developed in our lab. The shell formation conditions will be thoroughly investigated so that future work can focus on integrating Pd NPs synthesis [51–53] with the coating process. Initial work focused on directly translating the batch process to flow conditions, but these conditions resulted in poor material properties and reactor clogging issues. These issues were resolved through investigating the batch synthesis of Pd@TiO_2, including several parameters such as the concentration of the precursors [11]. After identifying favorable

conditions for batch synthesis, these changes were implemented to the continuous jet-mixing process, including modifying the reactor to limit pre-mature hydrolysis of the titania precursor. The Pd@TiO_2 nanomaterials are synthesized via batch and jet-mixing and their properties are compared. Additionally, the materials synthesized via batch and jet-mixing are tested for the HDO of benzyl alcohol to evaluate their catalytic performance. Overall, this work demonstrates the use of the jet-mixing reactor for the scalable and continuous synthesis of inverted nanomaterials.

2. Results and Discussion

2.1.Pd NP synthesis

Pd NPs are synthesized in batch mode by reducing $Pd(acac)_2$ by oleylamine in the presence of TOP as capping ligand at 220°C. The procedure for generating the metal center of the catalyst results in successful Pd NP synthesis, as is indicated by characterization with XRD. The XRD pattern obtained for a representative as-synthesized Pd NP batch is shown on the right side in Figure 1. Peaks corresponding to the (111), (200), (220) and (311) diffraction planes of Pd can be identified in the pattern. Additionally, broadening of the peaks is observed. These observations suggest the presence of Pd NPs in the resultant material. TEM analysis is used on some of the samples to determine the particle size. Several images from different grid locations are taken, one of which is shown in Figure 1. The size of around 100 particles is measured using ImageJ software [54] and it is determined that the average size of Pd NPs is 7±2 nm, as shown in the top-left inset in Figure 1.

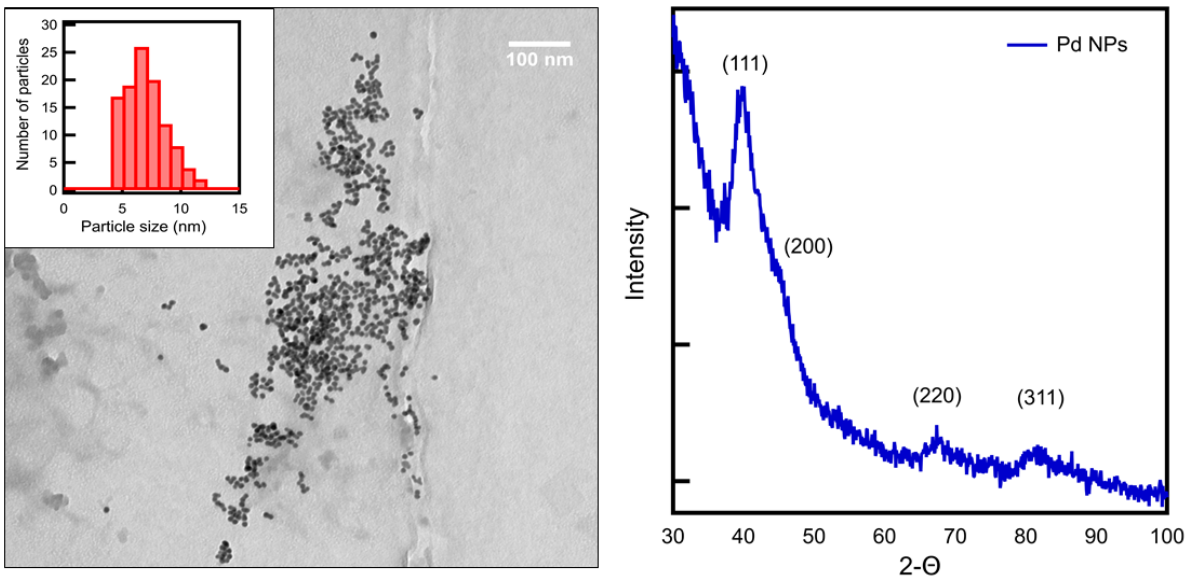

Fig 1 TEM image of as-synthesized Pd NPs, synthesized by the reduction of $Pd(acac)_2$ at 220 °C in the presence of OA, using TOP as the capping agent. The inset on the top left shows the particle size distribution obtained through TEM. The sizes of over 100 particles from different grid locations are measured via ImageJ software to calculate the size distribution. The average particle size is 7±2 nm. (Right) XRD data for the batch synthesis of Pd NPs, including peak labels for the diffraction plane.

The nature of capping on the surface of the Pd NPs is determined by analyzing the synthesized materials with FTIR-ATR. The spectra for the batches are shown in Figure S1a. The spectra have many features including the stretching bands around 2950 cm^{-1}, 2915 cm^{-1}, 2868 cm^{-1}, and 2846 cm^{-1} that suggest the presence of C-H bonds on the surface. The C-H stretching bonds indicate that TOP, OA, or both (TOP and OA) molecules are present on the surface. The Pd NPs are also analyzed by FTIR-ATR post treating with CTAB. The spectrum obtained is shown in Figure S1b along with a spectrum for the pre-CTAB treated Pd NPs as a comparison. The spectrum for the post-treated material shows a stretching band at 1266 cm^{-1}, suggesting the presence of C-N bonds on the surface. This band is absent in the pre-treated Pd NP sample, suggesting successful encapsulation with CTAB. The inset on the bottom left of Figure S1b shows stretching bands associated with C-H bonds for both spectra, suggesting that some TOP is still present on the Pd NP surface post-CTAB treatment. The Pd NPs are also analyzed by SEM-EDS after adding CTAB

to confirm the presence of both TOP and CTAB on the surface. The EDS spectrum obtained for the material is shown in Figure S2. The presence of bromine and phosphorous is clearly observed, confirming CTAB and TOP surface capping, respectively.

2.2.Direct translation of batch method to jet-mixing reactor

Initial efforts are aimed at direct translation of the sol-gel batch synthesis procedure used in previous studies to a continuous process with the goal of achieving a material with high microporosity, as microporosity has been associated with increased selectivity towards HDO [17]. The effect of several synthesis parameters such as the nature of hydrolysis precursor, solvent, interfacial ligand concentration, and solution pH on the titania microporosity has been studied in literature [11]. The synthesis conditions that yield the highest microporosity among the tested parameters are selected for the standard synthesis. An adaptation of the batch synthesis involves the injection of ammonium hydroxide (1 mL) to a solution of CTAB-capped Pd NPs (7.6 mg) with $Ti(OBu)_4$ (2 mL) in ethanol (20 mL). Initially, a jet-mixing synthesis is set up with the solution containing Pd NP and $Ti(OBu)_4$ (20 mL) being delivered through the main line at 48 mL/h and ammonium hydroxide (20 mL) through the jet line at 48 mL/h. The volume of ammonium hydroxide is maintained equal to the $Ti(OBu)_4$ solution volume to allow for equal flowrates of the jet and main lines. Whereas the reactor could be operated with unequal flowrates, this work will focus on equal main and jet line flowrates since we have experience with equal flow rates in our previous work for nanomaterial synthesis using jet-mixing [32,50]. The reagent concentrations used in the jet-mixing synthesis are comparable to the batch.

The product collected from the jet-mixing run (material Pd@TiO_2-JM-neat NH_4OH) is characterized for microporosity via nitrogen physisorption. The pore size distribution obtained from the physisorption isotherm is shown in Figure 2, and the isotherm is shown in Figure S3. It

188 is observed that the material is largely mesoporous, as is seen by the hysteresis loop between
189 relative pressure (P/P_0) values of 0.4 to 1 in the isotherm. This can be visualized by the pore size
190 distribution that shows a high incremental pore volume for pores greater than 5 nm. However, the
191 ideal material for HDO is expected to have high microporosity with presence of mesopores in the
192 2-5 nm region. The JM set-up also clogs, leading to isolation of a small amount of product.

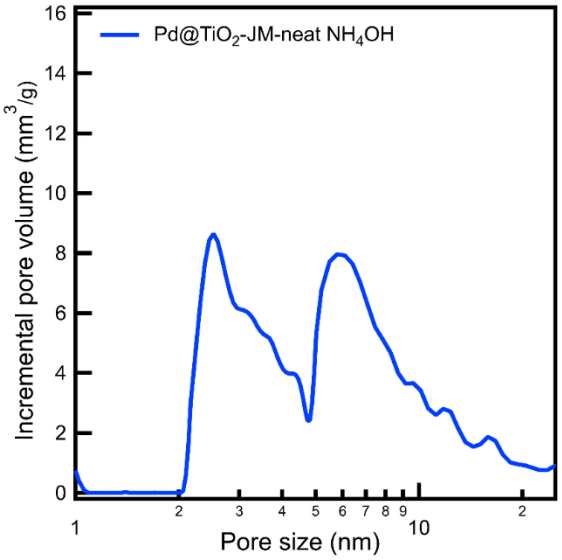

Fig 2 Nitrogen physisorption pore size distribution of $Pd@TiO_2$ synthesized by direct translation of the batch synthesis process to jet-mixing (material $Pd@TiO_2$-JM-neat NH_4OH). The main line carries Pd NPs and $Ti(OBu)_4$ in EtOH at 48 mL/h while the jet line carries ammonium hydroxide at 48 mL/h. Equimolar reagent quantities are used for the batch and jet-mixing syntheses.

193

194 Therefore, it is important to develop a synthesis procedure for the jet-mixing system after
195 examining the effect of synthesis parameters on the porosity and ease of operation. For adapting
196 the batch synthesis to a continuous system, the effects of several system parameters are
197 investigated, including (1) the effect of dilution of reagent solutions, (2) the time delay between
198 addition of reagents, (3) rate of addition of titanium precursor.

199 **2.3. Dilution of ammonium hydroxide**

The original batch process involves the injection of a small volume of undiluted ammonium hydroxide in a short time period into the solution containing Pd NPs and $Ti(OBu)_4$. Since titanium precursor hydrolysis is a fast mixing-limited process, it is important that the ammonium hydroxide is injected in a controlled manner to control the material porosity [30]. The injection of a small volume of reagent into a significantly larger fluid volume over a burst of time may induce uncontrolled condensation because of poor mixing. The condensation process can be slowed by diluting the ammonium hydroxide [55]. This can be achieved by maintaining equal solution volumes of the ammonium hydroxide and the Ti-precursor solution while keeping total solvent volume constant. The total solvent volume in the system remains constant during this modification such that the concentrations of the ammonium hydroxide and Ti-precursor post-mixing are unchanged. Further, our previous work has investigated the synthesis of nanomaterials using equal reagent flowrates to limit the parameter space [32,50]. Future work will examine the effect of unequal flows in the jet and main lines.

The effect of dilution of the ammonium hydroxide on the porosity is examined. The original synthesis consists of the injection of ammonium hydroxide, Solution B (1 mL) into a solution of Pd NPs and $Ti(OBu)_4$ in ethanol, Solution A (40 mL). In the modified synthesis, Solution B is diluted with ethanol while keeping the total ethanol volume in the system (40 mL) unchanged to ensure the reagent concentrations after mixing are comparable to the original batch. This is done by combining half of the ethanol volume (20 mL) with the ammonium hydroxide (1 mL) to make Solution B. The other half of the volume of the ethanol is added to the Pd NPs and $TiOBu_4$ to make Solution A. The ethanol used to prepare Solution A is anhydrous to prevent premature $Ti(OBu)_4$ hydrolysis.

Two Pd@TiO_2 nanomaterials are synthesized in batch: a control material with neat ammonium hydroxide injection (material Pd@TiO_2-B-neat NH_4OH) and the modified material with diluted ammonium hydroxide injection (material Pd@TiO_2-B-diluted NH_4OH). The rate of injection of Solution B into Solution A is maintained constant (1 mL/s) in the modified synthesis. All other synthesis parameters including reagent quantities are also maintained constant.

The porosity of the two resultant materials is compared by analyzing them with nitrogen physisorption. The pore size distributions obtained from the physisorption isotherms are shown in Figure 3, and the isotherms are shown in Figure S4. It is observed from the isotherms that both materials have micropores as indicated by the nitrogen uptake in the relative pressure (P/P_0) region less than 0.1. However, there is higher uptake in the relative pressure region associated with mesopores and macropores ($P/P_0 > 0.4$) by the material synthesized with neat NH_4OH injection than in material synthesized with diluted injection. This is also depicted by the pore size distribution curves that suggest a higher incremental pore volume for pores larger than 5 nm in the sample synthesized with neat injection as compared to the sample synthesized with diluted injection. The average fraction of microporosity calculated for the samples, listed in Table S1, is twice for the sample with diluted NH_4OH injection than for the sample with neat NH_4OH injection. This result supports the hypothesis that the injection of a small volume of NH_4OH into a significantly larger volume of Solution B results in uncontrolled hydrolysis of the titania precursor, leading to large pores. It is important to note that the simultaneous increase in the Ti-precursor concentration with ammonium hydroxide dilution may also affect sol-gel kinetics and hence the material properties. Overall, this observation suggests that diluting the ammonium hydroxide increases the fraction of microporosity in the synthesized Pd@TiO_2 material as compared with a

neat injection. Hence, dilution of the ammonium hydroxide in Solution B prior to injecting in Solution A is incorporated into the standard batch synthesis.

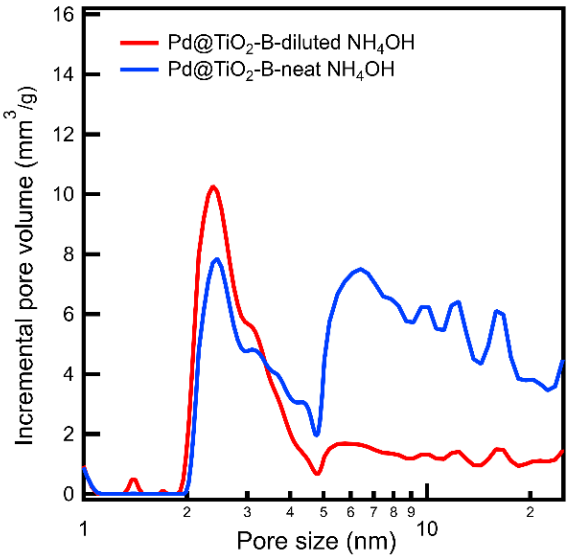

Fig 3 Nitrogen physisorption pore size distributions of Pd@TiO_2 nanomaterials synthesized using different dilutions of the ammonium hydroxide in Solution B. The amount of ethanol used to dilute the ammonium hydroxide is varied from 20 mL in material Pd@TiO_2-B-diluted NH_4OH (red line) to 0 mL in material Pd@TiO_2-B-neat NH_4OH (blue line). The total amount of ethanol in each system is maintained at 40 mL. All other synthesis parameters including reagent quantities and injection rates are maintained the same in the two syntheses

2.4. Aging time of Ti precursor in solvent

Solution A is prepared by the addition of $Ti(OBu)_4$ to a suspension of Pd NPs in ethanol. However, the addition of $Ti(OBu)_4$ to ethanol can result in its alcoholysis by alkoxy group exchange, because of the presence of ethoxy groups in the reaction medium [56]. This likely results in the formation of $Ti(OBu)_x(OEt)_{4-x}$ species in solution. In literature, the nature of the Ti precursor species formed because of alcoholysis has been suggested to directly influence the rates of hydrolysis and condensation of titania, influencing its properties [11,57]. The extent to which the alcoholysis reaction sequence proceeds before hydrolysis occurs would depend on the aging time

of $Ti(OBu)_4$ in ethanol, prior to the addition of the ammonium hydroxide. If the duration of contact between the $Ti(OBu)_4$ and ethanol has an effect on the material porosity, the jet-mixing system will have to be designed such that the residence time between $Ti(OBu)_4$ addition and ammonium hydroxide addition is controlled. This may require a modified jet-mixing geometry, with three separate inlets for the Ti-precursor, Pd NP-containing ethanol, and the ammonium hydroxide. Hence, the effect of the aging time of $Ti(OBu)_4$ in ethanol on the Pd@TiO_2 microporosity are examined before designing the jet-mixing system.

Solution A and Solution B are prepared according to the standard batch synthesis procedure. Two Pd@TiO_2 materials are synthesized in batch with different time intervals between the formation of Solution A, and the addition of Solution B to Solution A. The time interval is varied from 15 seconds (material Pd@TiO_2-B-t(Ti-NH_4OH)-15s) to 30 minutes (material Pd@TiO_2-B-t(Ti-NH_4OH)-30min). All other synthesis parameters are maintained constant.

The products are isolated and analyzed with nitrogen physisorption to determine their porosity. The pore size distributions obtained for the materials are plotted in Figure 4, and their physisorption isotherms are shown in Figure S5. The isotherms and pore size distributions for both materials overlap with each other, suggesting there is no difference in the porosity. The results for both materials indicate the presence of micropores and small mesopores between 2-5 nm, consistent with Pd@TiO_2 syntheses under similar conditions in literature [11]. The average fraction of microporosity in the materials, listed in Table S2, is comparable for both materials. This suggests that a $Ti(OBu)_4$ aging time period in ethanol in the range of 15 seconds to 30 minutes prior to ammonium hydroxide addition has no effect on the material porosity. Hence, a 30-minute time period is arbitrarily chosen as the synthesis parameter for the standard batch synthesis. This result does not require additional modifications of the jet-mixing reactor.

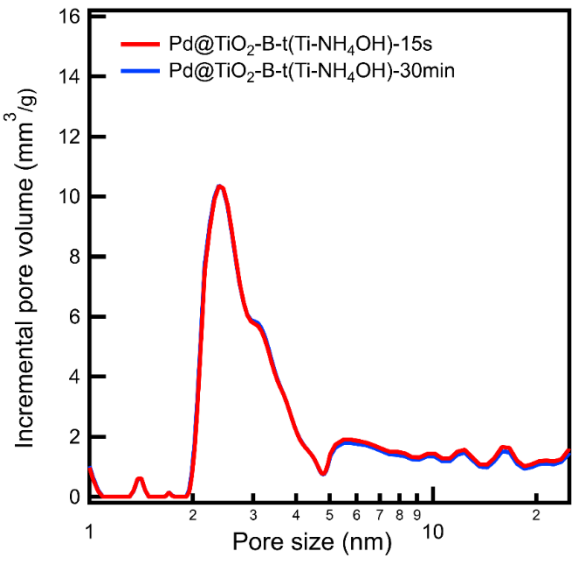

Fig 4 Nitrogen physisorption pore size distributions of $Pd@TiO_2$ nanomaterials synthesized with different aging times of $Ti(OBu)_4$ in ethanol, prior to the addition of the the ammonium hydroxide. The time interval is varied from 15 seconds in material $Pd@TiO_2$-B-t(Ti-NH_4OH)-15s (red line) to 30 minutes in material $Pd@TiO_2$-B-t(Ti-NH_4OH)-30min (blue line). All other synthesis parameters including reagent quantities and injection rates are maintained the same in the two syntheses.

2.5. Rate of injection of Ti precursor

An important consideration in the preparation of Solution A is the rate of addition of $Ti(OBu)_4$ to Pd NPs suspended in ethanol. The rate at which the ammonium hydroxide is added to the Ti-precursor has been shown to affect the porosity in the resultant TiO_2 phase. [17,30] However, the rate of injection of the Ti precursor into the Pd NPs suspension in ethanol has yet to be investigated. As described in the previous section, addition of $Ti(OBu)_4$ to EtOH results in alcoholysis of the Ti precursor by the ethoxy groups to form $Ti(OBu)_x(OEt)_{4-x}$ species. An uncontrolled injection of the Ti precursor into the ethanol may lead to uncontrolled rates of alcoholysis of $Ti(OBu)_4$ and finally affect the properties of the TiO_2 phase. The rate of addition may also impact the nature of the interaction between the Ti-groups and the CTAB on the surface of the Pd NPs. It is hence important to investigate the effect of the rate of injection of Ti precursor

into the Pd NPs suspension while preparing Solution A. Two Pd@TiO_2 materials are synthesized in batch with different rates of addition of $Ti(OBu)_4$ into the suspended Pd NPs. One is synthesized with an instantaneous rate of injection of $Ti(OBu)_4$ (0.2 mL/s; material Pd@TiO_2-B-Ti-0.2mL/s) and another with a slow dropwise rate of injection (0.006 mL/s; material Pd@TiO_2-B-Ti-0.006mL/s). All other reagent concentrations, volumes and synthesis procedures are maintained constant. The porosities and pore size distribution of the resultant materials are obtained through nitrogen physisorption. The pore size distributions are plotted in Figure 5 and isotherms in Figure S6. The plots for both materials overlap with each other, indicating that there is no difference in the porosities of the materials synthesized. Both materials suggest the presence of micropores and small mesopores in the 2-5 nm region, consistent with Pd@TiO_2 syntheses under similar conditions in literature [11]. The values for average % microporosity that are listed in Table S3 in the SI are comparable for both materials. This suggests that the rate of addition of $Ti(OBu)_4$ to the Pd NPs suspension does not have an effect on the porosity of the TiO_2 phase formed. Hence, an arbitrary rate of $Ti(OBu)_4$ injection of 0.2 mL/s is chosen as the synthesis parameter for standard batch and JM syntheses.

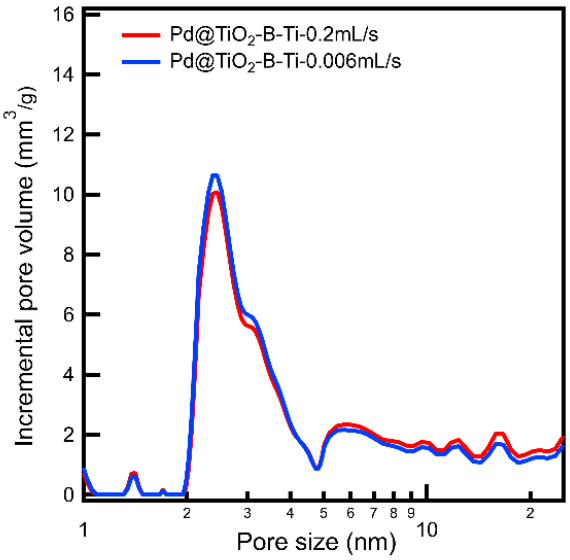

Fig 5 Nitrogen physisorption pore size distributions of Pd@TiO_2 nanomaterials synthesized using different rates of injection of $Ti(OBu)_4$ to the Pd NPs suspension in the standard batch synthesis. The rate of injection is varied from 0.2 mL/s in material Pd@TiO_2-B-Ti-0.2mL/s (red line) to 0.006 mL/s in material Pd@TiO_2-B-Ti-0.006mL/s (blue line). All reagent quantities and other procedures are maintained the same in the two syntheses.

Overall, the results from these batch tests are used to synthesize a final batch of Pd@TiO_2 to compare with the materials made using the jet-mixing reactor. As dilution of the ammonium hydroxide reduces the mesoporosity in the material, all standard syntheses are done by diluting the ammonium hydroxide with half the total solvent volume in the system. Further, since there is no effect of the alcoholysis side-reaction between $Ti(OBu)_4$ and ethanol on the porosity, they are mixed prior to the jet-mixing run, eliminating the need for a geometry with a separate inlet for the $Ti(OBu)_4$. The experimental parameters that are chosen to develop the standard batch synthesis are listed in Table S4. The standard batch synthesis is then directly translated to develop the jet-mixing process.

2.6. Standard batch and jet-mixing Pd@TiO_2 syntheses

316 Pd@TiO_2 nanomaterials are synthesized at comparable reagent concentrations using batch
317 (material Pd@TiO_2-B) and jet-mixing (material Pd@TiO_2-JM), and their properties are compared.
318 In a mixing-limited system, the properties of the resultant material are expected to depend on the
319 mixing time as the base-catalyzed hydrolysis of the $Ti(OBu)_4$ is reported to be a fast process [33].
320 An estimate of the mixing time scale for the jet mixing reactor derived from our previous work
321 suggests that it is at least two orders of magnitude smaller than that for a batch process [32].
322 Whereas the properties of the materials produced using the jet-mixing reactor would be expected
323 to be equal to or better than the properties of materials made using a scaled-up batch process, the
324 microporosity obtained from both the batch and jet-mixing processes is expected to be comparable
325 since the batch method is performed at small scale.

326 Pd@TiO_2 nanomaterials synthesized by standard batch and jet-mixing processes are
327 analyzed by nitrogen physisorption, XRD, TEM and SEM-EDS. The pore size distributions
328 derived for the materials are plotted in Fig. 6 and their isotherms are shown in Figure S7. It is
329 observed in the isotherms that the uptake in the relative pressure region associated with micropores
330 ($P/P_0 < 0.1$) is similar in both materials. A slightly higher uptake is observed in the region
331 associated with mesopores and macropores ($P/P_0 > 0.4$) for the jet-mixing synthesized material as
332 compared to the batch-synthesized material. It is observed from the pore size distributions that a
333 higher incremental pore volume in the microporous region with pore size less than 2 nm is obtained
334 for the jet-mixing synthesized material as compared to the batch-synthesized material. However,
335 this is offset by the higher incremental pore volume in the pore size region greater than 5 nm,
336 showing the presence of greater mesopores, compared to the batch-synthesized material. These
337 results are consistent with our hypothesis that the reaction system is free of mass-transfer
338 limitations and results in a jet-mixing synthesized material that has properties comparable to the

batch-synthesized material. Interestingly, it is found that scaling-up the batch synthesis method by a factor of eight resulted in a material with reduced micropore volume (see supplemental information).

The crystal structure of the resultant TiO_2 is analyzed by XRD and the diffraction spectra of both materials are shown in Fig. S8. From the broad peaks obtained over the range of diffraction angles from 20°-80°, it is concluded that amorphous titania is formed in both materials. This observation is consistent with results for Pd@TiO_2 material obtained at similar synthesis parameters in previous literature [11]. The samples are analyzed by TEM to check for Pd NP encapsulation in the TiO_2 phase. TEM images for the standard batch and jet-mixing synthesized Pd@TiO_2 materials are shown in Figures 7a and 7b respectively. The presence of Pd NPs is suggested by the dark-colored areas in the lighter-colored TiO_2 matrix. Both materials suggest a similar nature of Pd NP encapsulation by TiO_2. The samples are also analyzed by SEM-EDS to find the loading of Pd in the material. It is seen that the loading for both materials is ~0.7-0.9% Pd by weight. These results are supported by comparison with prior literature in which Pd@TiO_2 materials are synthesized under similar conditions. These studies also report a Pd loading between 0.7-1% for materials synthesized in ethanol using water to initiate $Ti(OBu)_4$ hydrolysis [11,17]. Overall, these analyses suggest that the Pd@TiO_2 materials synthesized in batch and jet-mixing are comparable in their properties. Hence, a scalable process has been developed for continuous Pd@TiO_2 synthesis while retaining the material quality obtained in a lab-scale batch.

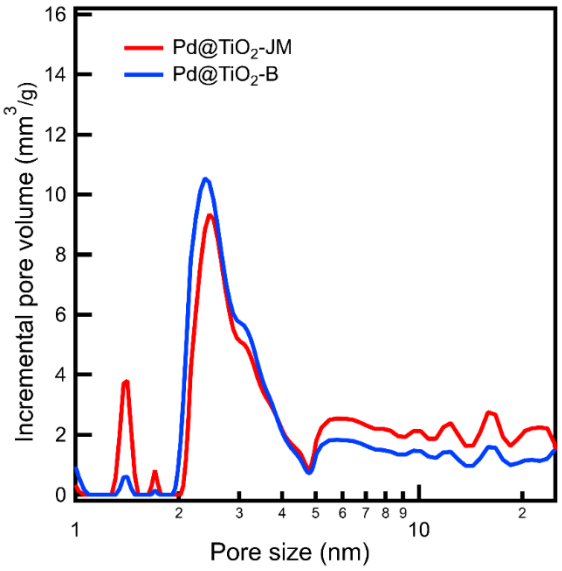

Fig 6 Nitrogen physisorption pore size distributions of Pd@TiO_2 nanomaterials synthesized using standard batch (material Pd@TiO_2-B) and standard jet-mixing (material Pd@TiO_2-JM) synthesis. The main line and jet line flowrate are maintained at 48 mL/h for the jet-mixing synthesis. All reagent quantities and concentrations are maintained the same in the two syntheses.

358

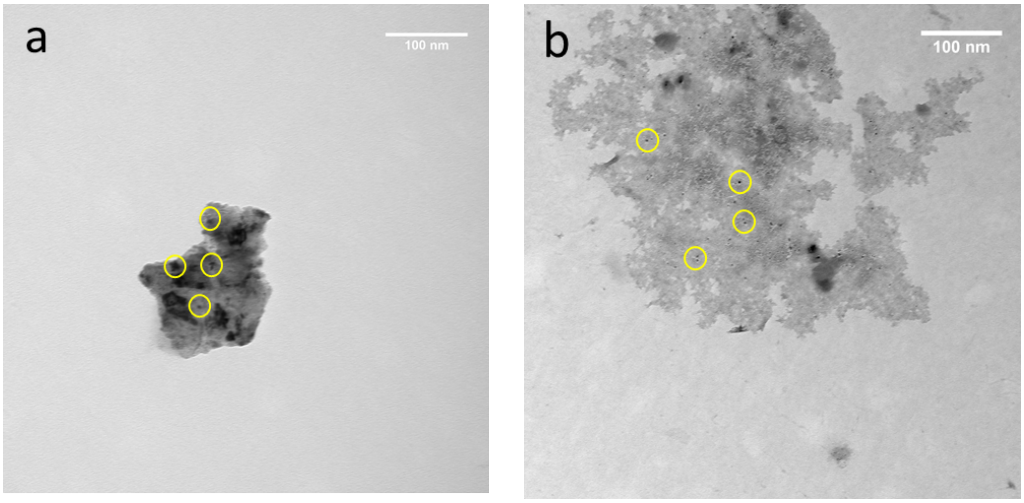

Fig 7 TEM images of Pd@TiO_2 nanomaterials synthesized by: (**a)** standard batch and (**b)** standard jet-mixing at a flow rate of 48 mL/h in the main and jet lines. The areas circled in yellow highlight some of the Pd NPs visible in the TiO_2 matrix. Both syntheses are done at comparable reagent concentrations.

359

360 2.7. Effect of jet-mixing flowrate

Flexibility of operation over a range of flowrates is an attractive feature of a continuous process. The flowrate in the jet-mixing reactor is varied to investigate its effect on the microporosity of Pd@TiO_2. Specifically, the rate of mixing in the system is expected to increase with an increase in flowrate, leading to fast hydrolysis of the titanium precursor and high microporosity. The total flowrate in the reactor is varied while maintaining equal flowrates in the main and jet lines. Three Pd@TiO_2 materials are synthesized by setting the flowrate in each line to 12 mL/h (material Pd@TiO_2-JM-12 mL/h), 48 mL/h (material Pd@TiO_2-JM-48 mL/h), and 200 mL/h (material Pd@TiO_2-JM-200 mL/h). The reagent concentrations for all syntheses are comparable to the batch-synthesized material. The materials are isolated and analyzed by nitrogen physisorption to obtain their microporosity. The pore distributions for the materials derived from the isotherms are shown in Figure 8, and the isotherms are shown in Figure S9. It is observed from the isotherms that the nitrogen uptake in the microporous region ($P/P_0 < 0.1$) increases with an increase in flowrate. This is corroborated by an increase in incremental pore volume in the micropore region (< 2 nm) with increasing flowrate. The micropore volumes obtained for the materials are shown in Table S5. The micropore volume for the sample synthesized at 12 mL/h is zero, suggesting the absence of micropores. The uptake in the mesopore region with pore size greater than 5 nm also increases with an increase in flowrate. These combined observations combined suggest that the microporosity obtained for the materials synthesized at 48 mL/h and 200 mL/h may be comparable. These materials are hence further selected for catalytic testing.

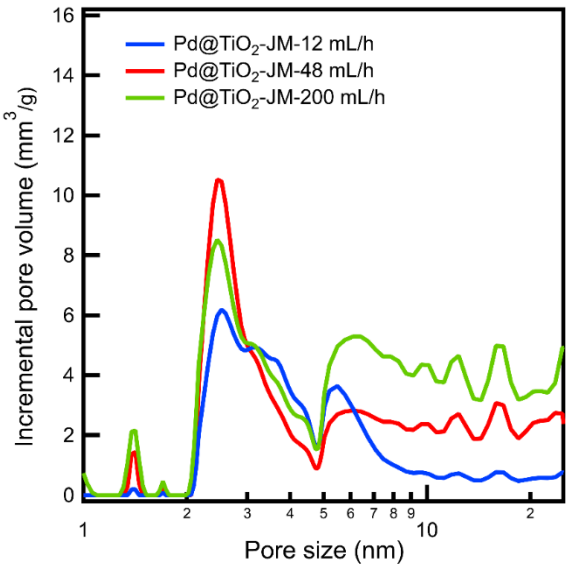

Fig 8 Nitrogen physisorption pore size distributions of Pd@TiO_2 nanomaterials synthesized at different jet-mixing flowrates. The flowrate in the main line is varied from 12 mL/h (material Pd@TiO_2-JM-12 mL/h) to 48 mL/h (material Pd@TiO_2-JM-48 mL/h) to 200 mL/h (material Pd@TiO_2-JM-200 mL/h). The flowrate in the jet line is maintained equal to that in the main line. Reagent concentrations for all synthesis are comparable to the standard batch synthesis.

380

381 **2.8. Catalytic testing for HDO of benzyl alcohol**

382 The Pd@TiO_2 nanomaterials synthesized via standard batch and at jet-mixing flowrates of
383 48 mL/h and 200 mL/h are tested for the hydrodeoxygenation (HDO) of benzyl alcohol. HDO of
384 benzyl alcohol can produce either the desired product toluene via the hydrodeoxygenation pathway
385 or the undesired product benzene via the decarbonylation pathway. The reaction scheme is shown
386 in Scheme 1. Previous literature has studied the activity of Pd@TiO_2 catalysts for the HDO of
387 aromatics in which hydrogenation is an unfavorable potential pathway, [11,17] finding that the
388 extent of microporosity of the titania framework in the catalyst determines the dominant reaction
389 pathway. As the characterization data of the batch and jet-mixing synthesized Pd@TiO_2 indicate
390 a comparable density of micropores in both materials, it is expected that both materials will exhibit

391 similar selectivity towards HDO, which would be a higher selectivity towards toluene as compared
392 to benzene.

393 The selectivity and activity for all materials are compared after 2 hours of time on-stream.
394 For this work, the conversion for each run is controlled at approximately 3.5%. EDS indicated that
395 samples made using the methods in this work contained a Pd loading of 0.76%. Using this loading,
396 the mass of catalyst used, reactant flowrate, and product yields, the normalized rate of production
397 for toluene and benzene was calculated. Figure 9 depicts these rates of production for the catalysts
398 used in the current work, as well as a comparison to previous work. As could be expected, the
399 catalyst produced using the batch method in this work could achieve a high selectivity to the HDO
400 reaction product toluene. Indeed, there is no detection of the decarbonylation product benzene.
401 From the GC detection limit for benzene at the conversions used, the minimum selectivity for
402 toluene is calculated as 99.3%. The increased HDO performance has been attributed to maximizing
403 interfacial contact between metal and metal oxide sites and restricting the accessible conformations
404 of benzyl alcohol on the surface, as reported in the previous work [17]. In addition to toluene, it
405 is found that a portion of the benzyl alcohol is converted to benzaldehyde, which is in equilibrium
406 with benzyl alcohol. These results are similar, within experimental uncertainty, to the materials
407 produced with batch methods where water was added instantaneously (i.e., Pd@TiO_2-WI) reported
408 in the previous work [11,17] and better in terms of selectivity than materials made through
409 dropwise addition of the water (Pd@TiO_2-WD), which had an HDO selectivity of 84% both of
410 which were reported in previous work [11,17]. The similar HDO performance between catalysts
411 in this work and catalysts from prior work demonstrate that the quality of catalyst is not
412 compromised under the improved synthesis procedures. All catalysts synthesized yielded better
413 HDO performance compared to an unmodified Pd/TiO_2 catalyst prepared via incipient wetness

414 impregnation (Pd/TiO_2-IWI), which gave a lower rate of toluene production and toluene selectivity
415 of only ~50%.

416 Figure 9 also depicts the conversion and production rate values for materials made using
417 the JMR at flow rates of 48 mL/h and 200 mL/h. At similar values of benzyl alcohol conversion
418 (~3.5%), the selectivity values for materials made using the JMR are similar to the values for
419 materials made using batch methods. Overall, these results indicate that the $Pd@TiO_2$
420 nanocatalysts synthesized via continuous jet-mixing are highly selective towards the benzyl
421 alcohol HDO product (i.e., selectivity for toluene >99.3%). This demonstrates that the desired
422 inverted structure can be achieved using a continuous process. Additionally, the desired $Pd@TiO_2$
423 materials can be achieved over a range of flow rates. These results will be used as a basis for future
424 experiments that will integrate the high temperature production of palladium nanoparticles with
425 the shell process demonstrated in this work. The high flow rate results will be beneficial as
426 upstream processes combining precursors (i.e., Pd and Ti) will result in a high overall flow rate.
427 These results indicate that the JM reactor is capable of handling the broad range of potential
428 conditions.

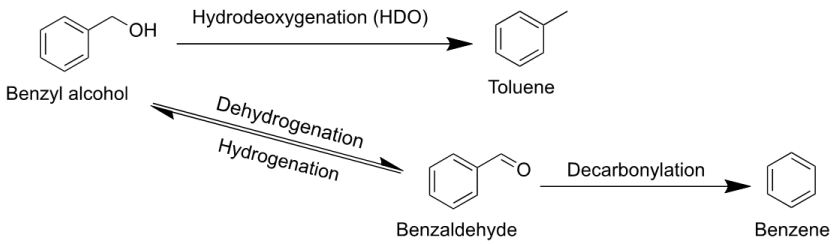

429

430 **Scheme 1.** Reaction scheme for benzyl alcohol hydrodeoxygenation (HDO). The desired reaction
431 pathway yields toluene whereas the undesirable decarbonylation pathway involves an equilibrium
432 between benzyl alcohol and benzaldehyde that can produce benzene.

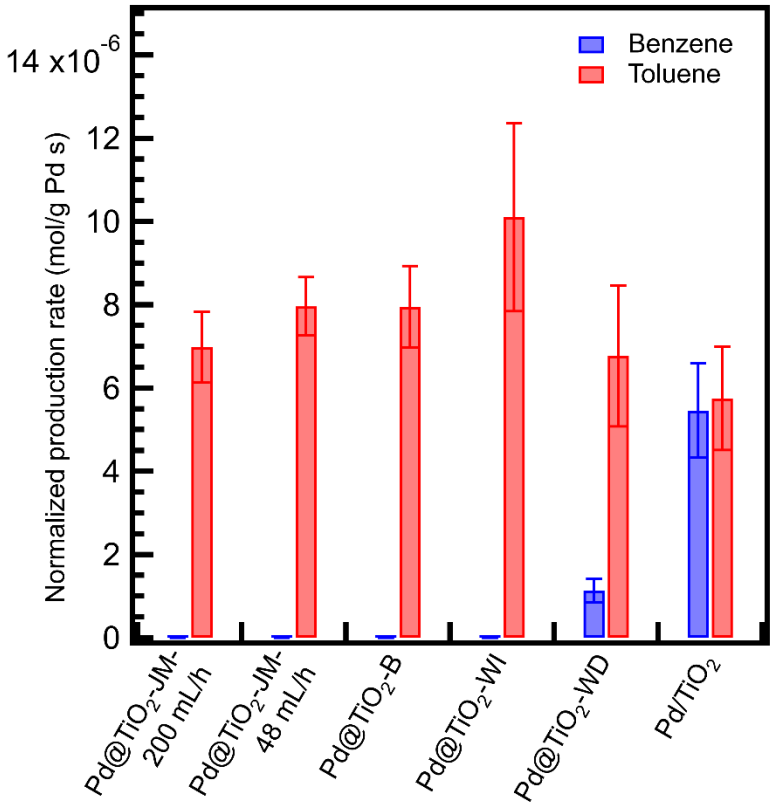

433

434 **Fig 9** Comparison of the normalized production rates obtained for Pd@TiO_2 materials synthesized in this
435 work using batch and jet-mixing (Pd@TiO_2-JM-200mL/h, Pd@TiO_2-JM-48mL/h, Pd@TiO_2-B), materials
436 prepared via batch methods in prior work (Pd@TiO_2-WI, Pd@TiO_2-WD) [11, 17], and Pd/TiO_2 prepared
437 via incipient wetness impregnation (Pd/TiO_2-IWI). For this work, the reactor is operated to achieve a
438 conversion of ~3.5%. The two jet-mixing synthesized materials tested are synthesized using flowrates of
439 48 mL/h and 200 mL/h respectively. Error bars represent s.d. of triplicate runs.

440 **3. Summary**

441 Pd@TiO_2 inverted nanocatalysts are synthesized in flow using a jet-mixing reactor.
442 Whereas the process identified previously could not be directly translated to a continuous process,
443 a series of batch experiments provided the necessary insights to create a continuous process.
444 Importantly, the jet-mixing reactor is modified to include a collection flask that can be maintained
445 under air-free conditions and the ammonia precursor is diluted with ethanol to slow the rate of
446 titanium precursor hydrolysis, which limited reactor clogging and created the desired
447 microporosity. It is observed that these materials produced using the jet-mixing reactor have a

448 microporosity comparable to their batch-synthesized counterpart. The catalytic activity of the
449 materials for the hydrodeoxygenation (HDO) of benzyl alcohol is tested. It is observed that the
450 material has a comparable selectivity for HDO products than its batch-synthesized counterpart.
451 Overall, it is demonstrated that jet-mixing is a scalable technique to produce Pd@TiO_2 inverted
452 nanocatalysts in a continuous manner while maintaining properties obtained in a lab-scale batch
453 reactor.

454 ## 4. Experimental Methods

455 ### 4.1.Chemicals

456 All chemicals are used as received without further purification, including: Palladium acetyl
457 acetonate ($Pd(acac)_2$, 99%, Sigma Aldrich), oleylamine (OA, technical grade, 70%, Sigma
458 Aldrich), trioctylphosphine (TOP, 97%, Sigma Aldrich), titanium (IV) butoxide ($Ti(OBu)_4$, reagent
459 grade, 97%), ammonium hydroxide aqueous solution (28-30% by weight ammonia basis), ethanol
460 (200 Proof, Decon Laboratories), anhydrous ethanol (99.5% anhydrous, 200 Proof, ACROS
461 organics), chloroform (≥99.7%, glass distilled, Electron Microscopy Sciences), hexanes (ACS
462 grade, ≥98.5%, BDH Chemicals), cetyltrimethylammonium bromide (CTAB, 99%, VWR
463 chemicals). The anhydrous ethanol, TOP, and $Ti(OBu)_4$ are stored under nitrogen in the glovebox.

464 ### 4.2.Reactor Design

465 The jet-mixing reactor geometry has been adapted from a reactor used for gas phase
466 synthesis [49] and has been previously used to demonstrate successful ZIF-8 and Ag NP synthesis
467 in the liquid phase by our group [32,50]. The reactor is manufactured in-house from a thermally
468 and chemically resistant polyether ether ketone (PEEK) cube (1” x 1” x 1”). The cube has two
469 cylindrical flow channels that intersect perpendicularly in the center. One flow channel is called

the main line and has a diameter (d_{main}) of 0.04 inch (~1000 μm) through the entire length of the cube. The other flow channel consists of a jet line with a diameter (d_{jet}) of 0.02 inch (~500 μm). The jet line is constructed such that two opposite-facing jets perpendicularly impinge the main line. Although the jets impinge from opposite sides of the main line, the jet-mixing reactor is manufactured by drilling both jet lines from one side of the cube for alignment purposes. The channels are threaded at the ends for connecting clear polytetrafluoroethylene (PTFE, ID 0.03") tubing using microfluidic PEEK fittings of appropriate size. The reactants are pumped using two KD Scientific 100KD syringe pumps through the tubing. The jet line from the syringe pump is split into two lines, each of which connects to one of the jets. The combined jet lines and main line flows comprise the product solution that flows out of the reactor collinear to the main line.

4.3.Batch synthesis of Pd NPs

Batch methods are used to produce the Pd NPs that will form the metal center of the catalyst. The procedure used has been modified from previous syntheses [11,58]. $Pd(acac)_2$ is used as the palladium source along with OA acting as both the solvent and the reducing agent and TOP as the capping ligand. The molar quantities of the reagents used have been specified in Table S1. OA (9 mL) is used to dissolve $Pd(acac)_2$ (0.099 g) in a 25 mL 2-neck round bottom flask with a 0.4" hexagonal Teflon stir bar. The solvent is degassed for an hour and the system purged with nitrogen to yield an air-free atmosphere prior to the addition of TOP (0.06 mL), as TOP readily oxidizes to trioctylphosphine oxide in the presence of oxygen. The temperature of the system is maintained at 220°C using a heating mantle and a temperature controller. This temperature is selected based on optimum particle size of Pd NPs for hydroisomerization reactions and to prevent TOP degradation [11]. Once air-free conditions and a stable temperature are obtained, the TOP is injected rapidly into the flask. Stirring is maintained at 200 RPM and the system is held at 220°C

for an hour. The black particles obtained are separated by adding 25 mL reagent alcohol and centrifuging at 9000 RPM for 30 minutes. The particles are washed thrice before being rotovaped to dryness.

4.4.Standard batch synthesis of Pd@TiO_2

The batch-synthesized Pd NPs are coated with TiO_2 post characterization in a seeded growth synthesis by adapting a previously reported sol-gel synthesis [11]. First, the Pd NPs are capped by a hydrophilic surfactant CTAB to disperse them in ethanol. In a 50 mL two-neck round bottom flask, CTAB (0.088 g) is added, and the headspace purged with nitrogen for an hour to develop an air-free atmosphere. It is then dissolved in anhydrous ethanol (20 mL). The Pd NPs (7.6 mg) are dispersed in chloroform (2.98 g) and sonicated for fifteen minutes. This suspension is then added dropwise to the ethanol and CTAB mixture over four minutes. The system is stirred at 800 RPM and heated to 45°C for eight minutes to coat the TOP-capped Pd NPs with a layer of CTAB while evaporating chloroform. After cooling for 30 minutes, $Ti(OBu)_4$ (2 mL) is injected to form a mixture (Solution A) while stirring is maintained. Separately, ammonium hydroxide (1 mL) is mixed with ethanol (200 proof, 20 mL) to form Solution B. While stirring at 800 RPM, Solution B is rapidly injected into Solution A in a controlled manner within seven seconds. The step-wise schematic of the batch synthesis is shown in Figure 10a. The mixture is collected fifteen minutes post injection of Solution B and centrifuged at 9000 RPM for 10 minutes. The particles obtained are washed thrice using 20 mL of a volumetric mixture of 1:1 methanol and water before drying for 24 hours at 80°C.

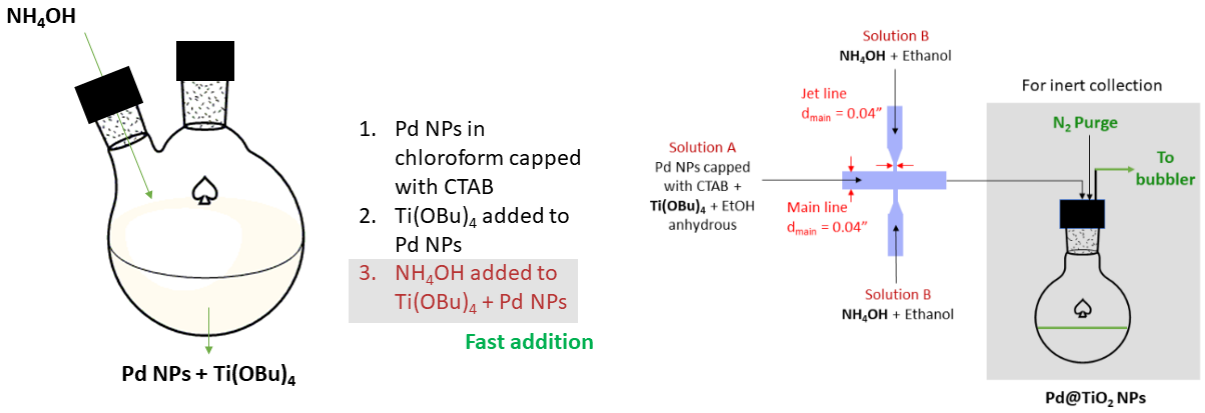

Fig 10a Schematic showing the step-wise procedure of the standard batch synthesis of Pd@TiO_2 starting from the addition of Pd NPs to the CTAB solution to the formation of Pd@TiO_2. The addition of NH_4OH to $Ti(OBu)_4$ is required to be fast for high microporosity. **10b** Schematic showing the design and set-up of the jet-mixing reactor for air-free synthesis of Pd@TiO_2. The main line ($d_{main} = 0.04$") and the jet line ($d_{jet} = 0.02$") carry Solutions A and B, respectively. The jets impinge perpendicularly on the main line to give the product stream. Solution A carries the Pd NPs with $Ti(OBu)_4$ while Solution B carries NH_4OH. The entire assembly is under air-free conditions because of the constant nitrogen purge through the septum attached to the collection flask. The Pd@TiO_2 is collected in the air-free collection flask downstream

4.5. Standard jet-mixing synthesis of Pd@TiO_2

Jet-mixing synthesized Pd@TiO_2 nanomaterials are prepared at concentrations of reagents comparable to the batch-synthesized counterpart. Solution A and Solution B are prepared in the same manner as for the batch synthesis and are filled into 60 mL BD Luer-Lok syringes. Before drawing out Solution A, the syringe is initially filled with nitrogen. It is important to ensure the jet-mixing assembly is under air-free conditions to prevent premature hydrolysis of the Ti precursor and to ensure the titania is deposited selectively around the Pd NPs. The JM assembly is modified to account for this, and a schematic of the design and set-up is shown in Figure 10b. The outlet tubing of the reactor is connected to the round-bottom flask in which the product is collected in an air-free manner. Initially, the syringe adapters are connected to the main and jet line tubing without connecting the reactant syringes. This entire assembly is purged with nitrogen before starting the jet-mixing experiment. This is done by initially passing a nitrogen purge Schlenk line

through the rubber septum and allowing the nitrogen to exit the jet-mixing system through the syringe adapters. In this manner, purging is done for 1.5 hours before the run. While the system is still being purged, the Solution A-containing syringe is connected to the main line and the Solution B-containing syringe to the jet line. Both syringe pumps are set to a flowrate of 48 mL/h, as we have previously used these flowrates for synthesis of Ag and ZIF-8 NPs [32,53]. The product Pd@TiO_2 is collected until the solutions are consumed. After collection, the Pd@TiO_2 mixture is immediately washed thrice using 20 mL of a volumetric mixture of 1:1 methanol and water before drying for 24 hours at 80°C.

4.6.Material Characterization

After drying, the Pd NPs are characterized via X-Ray Diffraction (XRD), Transmission Electron Microscopy (TEM), Fourier-transform Infrared Spectroscopy Attenuated Total Reflection (FTIR-ATR), and Scanning electron microscopy – energy dispersive X-ray spectroscopy (SEM-EDS). A Bruker D8 Advance X-ray powder diffractometer is used for XRD measurement. The diffraction spectra are collected using monochromatic Cu Kα1 radiation (λ = 1.54 Å) at 40 kV and 40 mA in Johannson mode. Pd NP samples are prepared by dissolving the dried NPs in ethanol and depositing a thin layer on the sample holder. Pd@TiO_2 samples are packed into the sample holder while ensuring the surface of the material remains flat. TEM has been used to characterize Pd NP size. For TEM, an FEI Tecnai G2 Spirit TEM at a voltage of 80 kV and magnification of either 1170,000x or 115,000x in bright-field mode has been used. FTIR-ATR and SEM-EDS have been used to check the binding of capping agents on the Pd NP surface. FTIR-ATR is performed using a Nicolet iS50 spectrophotometer. SEM-EDS has been performed using a ThermoFisher Apreo LoVac field emission SEM operating at 20 kV and spectroscopy data

is collected with an EDAX Octane Elect Plus 30 mm^2 EDS detector. EDAX TEAM software is used for analysis.

The Pd@TiO_2 nanomaterial is characterized via nitrogen physisorption, XRD, TEM, and SEM-EDS. Nitrogen physisorption is performed using a Micromeritics 3-Flex Surface Characterization analyzer to obtain adsorption isotherms from which pore size distributions and microporosity data of the Pd@TiO_2 materials can be extracted. Before analysis, samples are degassed for 24 hours at 80°C and for an additional 4 hours *in situ* before analysis. Pore size distributions are obtained by a built-in DFT method based on oxide surfaces with cylindrical pores. The structure of the material is determined via XRD, using the same instrument specifications as for Pd NP characterization. The amount of Pd encapsulated in the material is found via SEM-EDS using the same instrument set-up as for the Pd NP samples. Confirmation of the Pd NP encapsulation via TEM is also performed on some samples. Additional sample preparation details are provided in the supplementary information in Sections S1 and S2.

4.7.Catalytic testing

The synthesized materials are evaluated for HDO of benzyl alcohol in a tubular packed bed flow reactor at 190°C and atmospheric pressure. Helium is bubbled through the liquid reactant (benzyl alcohol) heated in a water bath maintained at 53.1°C. This stream is mixed with H_2 and additional make-up helium prior to reaching the catalyst bed. The resulting stream has gas-phase mole fractions of Y_{H2} = 25% and $Y_{\text{benzyl alcohol}}$ = 0.053% with a total flowrate of 75 sccm. The mass of catalyst is controlled to obtain a conversion of 3.5% ± 0.5% with the data taken at 120 min on-stream. The reactor effluent is analyzed using an Agilent 7890A Gas Chromatograph equipped with an Agilent HP-5 capillary column and a flame ionization detector. The normalized rate of production is calculated by multiplying the product yield by the molar flowrate of benzyl alcohol

570 divided by the effective mass of Pd in the catalyst sample. To determine the selectivity
571 performance of the catalysts, we monitored the selectivity (S) for toluene over benzene, i.e.

572 $S = Z_{tol} / (Z_{tol} + Z_{benz})$.

573 Here, Z_{tol} and Z_{benz} correspond to the yields of toluene and benzene, respectively. The side product
574 benzaldehyde is not included in the selectivity calculation because prior work [59] has shown that
575 benzaldehyde formation is reversible under the reaction conditions, and therefore benzaldehyde
576 yield approaches zero as the reaction approaches full conversion of benzyl alcohol. In contrast,
577 formation of the other products is essentially irreversible under the reaction conditions.

578 **4.8.Naming convention**

579 All Pd@TiO_2 samples have been labeled as Pd@TiO_2-X-parameter tested, where 'X' refers
580 to the method of synthesis (X = 'B' is batch, X = 'JM' is jet-mixing). The text after 'X' refers to
581 the parameter that is varied, if any, while performing the synthesis while holding all other
582 parameters constant and consistent with the standard batch and/or jet-mixing synthesis procedure.
583 A summary of all the materials synthesized in this work along with their synthesis conditions is
584 provided in Table S6.

585 **Declarations**

586 **Funding**

587 PR, AS, and NAB acknowledge support from the National Science Foundation through
588 grant number CBET-1653587. ZB and JWM acknowledge support from the National Science
589 Foundation through grant number CHE-1900183. Some images presented in this report were
590 generated using the instruments and services at the Campus Microscopy and Imaging Facility, The

591 Ohio State University. This facility is supported in part by grant P30 CA016058, National Cancer
592 Institute, Bethesda, MD.

593 **Conflicts of Interest/Competing Interests**

594 Not applicable.

595 **Availability of data and material**

596 Raw data will be made upon request within the five year period. Materials will be made
597 available upon request while materials remain in our current supplies.

598 **Code availability**

599 Not applicable.

600 **Authors' contribution**

601 PR synthesized and characterized materials made using batch and jet-mixing processes.
602 ZB tested the materials for catalytic activity. AS characterized the materials with SEM EDS. WM
603 and NAB helped design experiments and interpret results. All authors contributed to writing the
604 manuscript.

605 **Acknowledgements**

606 The authors acknowledge Steve Boona and the Center for Electron Microscopy and
607 Analysis (CEMAS) at The Ohio State University, where electron microscopy was performed.

608 **References**

609 [1] S. Kim, E.E. Kwon, Y.T. Kim, S. Jung, H.J. Kim, G.W. Huber, J. Lee, Recent advances in
610 hydrodeoxygenation of biomass-derived oxygenates over heterogeneous catalysts, Green
611 Chem. 21 (2019) 3715–3743. doi:10.1039/c9gc01210a.

612 [2] A.M. Robinson, J.E. Hensley, J. Will Medlin, Bifunctional Catalysts for Upgrading of
613 Biomass-Derived Oxygenates: A Review, ACS Catal. 6 (2016) 5026–5043.

614 doi:10.1021/acscatal.6b00923.

615 [3] A. Hornés, A.B. Hungría, P. Bera, A. López Cámara, M. Fernández-García, A. Martínez-
616 Arias, L. Barrio, M. Estrella, G. Zhou, J.J. Fonseca, J.C. Hanson, J.A. Rodriguez, Inverse
617 CeO2/CuO catalyst as an alternative to classical direct configurations for preferential
618 oxidation of CO in hydrogen-rich stream, J. Am. Chem. Soc. 132 (2010) 34–35.
619 doi:10.1021/ja9089846.

620 [4] M. Cargnello, N.L. Wieder, T. Montini, R.J. Gorte, P. Fornasiero, Synthesis of dispersible
621 Pd@CeO2 core-shell nanostructures by self-assembly, J. Am. Chem. Soc. 132 (2010)
622 1402–1409. doi:10.1021/ja909131k.

623 [5] J. Lu, B. Fu, M. Kung, G. Xiao, J. Elam, H. Kung, P.C. Stair, Coking- and Sintering-
624 Resistant Palladium Catalysts Achieved Through Atomic Layer Deposition, Science (80-.
625). 335 (2012) 1205–1209.

626 [6] M. Cargnello, J.J. Delgado Jaén, J.C. Hernández Garrido, K. Bakhmutsky, T. Montini, J.J.
627 Calvino Gámez, R.J. Gorte, P. Fornasiero, Exceptional activity for methane combustion
628 over modular Pd@CeO2 subunits on functionalized Al2O3, Science (80-.). 337 (2012)
629 713–717. doi:10.1126/science.1222887.

630 [7] A. Robinson, G.A. Ferguson, J.R. Gallagher, S. Cheah, G.T. Beckham, J.A. Schaidle, J.E.
631 Hensley, J.W. Medlin, Enhanced Hydrodeoxygenation of m-Cresol over Bimetallic Pt-Mo
632 Catalysts through an Oxophilic Metal-Induced Tautomerization Pathway, ACS Catal. 6
633 (2016) 4356–4368. doi:10.1021/acscatal.6b01131.

634 [8] J. Zhang, J.W. Medlin, Catalyst design using an inverse strategy: From mechanistic
635 studies on inverted model catalysts to applications of oxide-coated metal nanoparticles,

636 Surf. Sci. Rep. 73 (2018) 117–152. doi:10.1016/j.surfrep.2018.06.002.

637 [9] T. Xu, C. Lin, C. Wang, D.L. Brewe, Y. Ito, J. Lu, Synthesis of supported platinum
638 nanoparticles from Li-Pt solid solution, J. Am. Chem. Soc. 132 (2010) 2151–2153.
639 doi:10.1021/ja909442c.

640 [10] S. Marre, K.F. Jensen, Synthesis of micro and nanostructures in microfluidic systems.,
641 Chem. Soc. Rev. 39 (2010) 1183–202. doi:10.1039/b821324k.

642 [11] B. Wang, J. Zhang, L.P. Herrera, J.W. Medlin, E. Nikolla, *110th Anniversary:* Fabrication
643 of Inverted Pd@TiO $_2$ Nanostructures for Selective Catalysis, Ind. Eng. Chem. Res. 58
644 (2019) 4032–4041. doi:10.1021/acs.iecr.8b05896.

645 [12] S. Iqbal, X. Liu, O.F. Aldosari, P.J. Miedziak, J.K. Edwards, G.L. Brett, A. Akram, G.M.
646 King, T.E. Davies, D.J. Morgan, D.K. Knight, G.J. Hutchings, Conversion of furfuryl
647 alcohol into 2-methylfuran at room temperature using Pd/TiO2 catalyst, Catal. Sci.
648 Technol. 4 (2014) 2280–2286. doi:10.1039/c4cy00184b.

649 [13] O.F. Aldosari, S. Iqbal, P.J. Miedziak, G.L. Brett, D.R. Jones, X. Liu, J.K. Edwards, D.J.
650 Morgan, D.K. Knight, G.J. Hutchings, Pd–Ru/TiO 2 catalyst – an active and selective
651 catalyst for furfural hydrogenation, Catal. Sci. Technol. 6 (2016) 234–242.
652 doi:10.1039/C5CY01650A.

653 [14] Y. Nakagawa, K. Tomishige, Total hydrogenation of furan derivatives over silica-
654 supported Ni-Pd alloy catalyst, Catal. Commun. 12 (2010) 154–156.
655 doi:10.1016/j.catcom.2010.09.003.

656 [15] E.J. Roberts, S.E. Habas, L. Wang, D.A. Ruddy, E.A. White, F.G. Baddour, M.B. Griffin,

J.A. Schaidle, N. Malmstadt, R.L. Brutchey, High-Throughput Continuous Flow Synthesis of Nickel Nanoparticles for the Catalytic Hydrodeoxygenation of Guaiacol, ACS Sustain. Chem. Eng. 5 (2017) 632–639. doi:10.1021/acssuschemeng.6b02009.

[16] M. Lu, H. Du, B. Wei, J. Zhu, M. Li, Y. Shan, C. Song, Catalytic Hydrodeoxygenation of Guaiacol over Palladium Catalyst on Different Titania Supports, Energy and Fuels. 31 (2017) 10858–10865. doi:10.1021/acs.energyfuels.7b01498.

[17] J. Zhang, B. Wang, E. Nikolla, J.W. Medlin, Directing Reaction Pathways through Controlled Reactant Binding at Pd – TiO 2 Interfaces, Angew. Chemie - Int. Ed. 56 (2017) 6694–6698. doi:10.1002/ange.201703669.

[18] Q. Zhang, I. Lee, J.B. Joo, F. Zaera, Y. Yin, Core-shell nanostructured catalysts, Acc. Chem. Res. 46 (2013) 1816–1824. doi:10.1021/ar300230s.

[19] S.T. He, Y.L. Liu, H. Maeda, Controlled synthesis of colloidal silver nanoparticles in capillary micro-flow reactor, J. Nanoparticle Res. 10 (2008) 209–215. doi:10.1007/s11051-008-9509-6.

[20] H. Hong, L. Hu, M. Li, J. Zheng, X. Sun, X. Lu, X. Cao, J. Lu, H. Gu, Preparation of Pt@Fe2O3 nanowires and their catalysis of selective oxidation of olefins and alcohols, Chem. - A Eur. J. 17 (2011) 8726–8730. doi:10.1002/chem.201003429.

[21] G. Li, Z. Tang, Noble metal nanoparticle@metal oxide core/yolk-shell nanostructures as catalysts: Recent progress and perspective, Nanoscale. 6 (2014) 3995–4011. doi:10.1039/c3nr06787d.

[22] J. Huang, Y. Sun, S. Huang, K. Yu, Q. Zhao, F. Peng, H. Yu, H. Wang, J. Yang, Crystal

engineering and SERS properties of Ag-Fe3O4 nanohybrids: From heterodimer to core-shell nanostructures, J. Mater. Chem. 21 (2011) 17930–17937. doi:10.1039/c1jm13045e.

[23] J. Zhang, Y. Liu, Y. Luo, The turbulent behavior of novel free triple-impinging jets with large jet spacing by means of particle image velocimetry, Chinese J. Chem. Eng. 24 (2016) 757–766. doi:10.1016/j.cjche.2016.04.022.

[24] J. Piella, A. Gónzalez-Febles, J. Patarroyo, J. Arbiol, N.G. Bastús, V. Puntes, Seeded-Growth Aqueous Synthesis of Colloidal-Stable Citrate-Stabilized Au/CeO2 Hybrid Nanocrystals: Heterodimers, Core@Shell, and Clover- And Star-Like Structures, Chem. Mater. 31 (2019) 7922–7932. doi:10.1021/acs.chemmater.9b02005.

[25] H.S. Chae, S.D. Kim, S.H. Piao, H.J. Choi, Core-shell structured Fe3O4@SiO2 nanoparticles fabricated by sol–gel method and their magnetorheology, Colloid Polym. Sci. 294 (2016) 647–655. doi:10.1007/s00396-015-3818-y.

[26] L. Mockus, J.J. Peterson, J.M. Lainez, G. V. Reklaitis, Batch-to-Batch Variation: A Key Component for Modeling Chemical Manufacturing Processes, Org. Process Res. Dev. 19 (2015) 908–914. doi:10.1021/op500244f.

[27] S. Mülhopt, S. Diabaté, M. Dilger, C. Adelhelm, C. Anderlohr, T. Bergfeldt, J. Gómez de la Torre, Y. Jiang, E. Valsami-Jones, D. Langevin, I. Lynch, E. Mahon, I. Nelissen, J. Piella, V. Puntes, S. Ray, R. Schneider, T. Wilkins, C. Weiss, H.-R. Paur, Characterization of Nanoparticle Batch-To-Batch Variability, Nanomaterials. 8 (2018) 311. doi:10.3390/nano8050311.

[28] R.L. Hartman, J.P. McMullen, K.F. Jensen, Deciding whether to go with the flow: Evaluating the merits of flow reactors for synthesis, Angew. Chemie - Int. Ed. 50 (2011)

700 7502–7519. doi:10.1002/anie.201004637.

701 [29] R. Mezaki, M. Mochizuki, K. Ogawa, Engineering Data on Mixing, Elsevier, 2000.
702 doi:https://doi.org/10.1016/B978-0-444-82802-6.X5000-6.

703 [30] W. Li, Z. Wu, J. Wang, A.A. Elzatahry, D. Zhao, A perspective on mesoporous TiO2
704 materials, Chem. Mater. 26 (2014) 287–298. doi:10.1021/cm4014859.

705 [31] K.F. Jensen, Flow Chemistry — Microreaction Technology Comes of Age, AIChE J. 63
706 (2017) 858–869. doi:10.1002/aic.

707 [32] P. Ranadive, A. Parulkar, N.A. Brunelli, Jet-Mixing for the Production of Monodisperse
708 Silver Nanoparticles Using Reduced Amounts of Capping Agent, React. Chem. Eng. 4
709 (2019) 1779–1789. doi:10.1039/c9re00152b.

710 [33] B.K. Johnson, R.K. Prud'homme, Chemical processing and micromixing in confined
711 impinging jets, AIChE J. 49 (2003) 2264–2282. doi:10.1002/aic.690490905.

712 [34] Brian K Johnson, R.K. Prud'homme, Flash NanoPrecipitation of Organic Actives and
713 Block Copolymers using a Confined Impinging Jets Mixer, Aust. J. Chem. (2003) 1021–
714 1024. doi:10.1071/CH03115.

715 [35] J. Zhang, K. Wang, A.R. Teixeira, K.F. Jensen, G. Luo, Design and Scaling Up of
716 Microchemical Systems: A Review, Annu. Rev. Chem. Biomol. Eng. 8 (2017) 285–305.
717 doi:10.1146/annurev-chembioeng-060816-101443.

718 [36] C. Zhao, L. He, S. Zhang, A.P.J. Middelberg, Nanoparticle synthesis in microreactors,
719 Chem. Eng. Sci. 66 (2011) 1463–1479. doi:10.1016/j.ces.2010.08.039.

720 [37] J.M. Lim, A. Swami, L.M. Gilson, S. Chopra, S. Choi, J. Wu, R. Langer, R. Karnik, O.C.

721 Farokhzad, Ultra-high throughput synthesis of nanoparticles with homogeneous size
722 distribution using a coaxial turbulent jet mixer, ACS Nano. 8 (2014) 6056–6065.
723 doi:10.1021/nn501371n.

724 [38] R. Baber, L. Mazzei, N.T.K. Thanh, A. Gavriilidis, An engineering approach to synthesis
725 of gold and silver nanoparticles by controlling hydrodynamics and mixing based on a
726 coaxial flow reactor, Nanoscale. (2017) 14149–14161. doi:10.1039/C7NR04962E.

727 [39] R. Baber, L. Mazzei, N.T.K. Thanh, A. Gavriilidis, Synthesis of silver nanoparticles in a
728 microfluidic coaxial flow reactor, RSC Adv. 5 (2015) 95585–95591.
729 doi:10.1039/c5ra17466j.

730 [40] A. Abou Hassan, O. Sandre, V. Cabuil, P. Tabeling, Synthesis of iron oxide nanoparticles
731 in a microfluidic device: Preliminary results in a coaxial flow millichannel, Chem.
732 Commun. (2008) 1783–1785. doi:10.1039/b719550h.

733 [41] I. Valente, E. Celasco, D.L. Marchisio, A.A. Barresi, Nanoprecipitation in confined
734 impinging jets mixers: Production, characterization and scale-up of pegylated nanospheres
735 and nanocapsules for pharmaceutical use, Chem. Eng. Sci. 77 (2012) 217–227.
736 doi:10.1016/j.ces.2012.02.050.

737 [42] R. Baber, L. Mazzei, N.T.K. Thanh, A. Gavriilidis, Synthesis of silver nanoparticles using
738 a microfluidic impinging jet reactor, J. Flow Chem. 6 (2016) 268–278.
739 doi:10.1556/1846.2016.00015.

740 [43] J. Saien, S.A.E. Zonouzian, A.M. Dehkordi, Investigation of a two impinging-jets
741 contacting device for liquid–liquid extraction processes, Chem. Eng. Sci. 61 (2006) 3942–
742 3950. doi:10.1016/j.ces.2006.01.034.

743 [44] L. Yu, Y. Pan, C. Wang, L. Zhang, A two-phase segmented microfluidic technique for
744 one-step continuous versatile preparation of zeolites, Chem. Eng. J. 219 (2013) 78–85.
745 doi:10.1016/j.cej.2013.01.009.

746 [45] H. Mehenni, L. Sinatra, R. Mahfouz, K. Katsiev, O.M. Bakr, Rapid continuous flow
747 synthesis of high-quality silver nanocubes and nanospheres, RSC Adv. 3 (2013) 22397.
748 doi:10.1039/c3ra43295e.

749 [46] L. Paseta, B. Seoane, D. Julve, C. Te, Accelerating the Controlled Synthesis of Metal −
750 Organic Frameworks by a Microfluidic Approach: A Nanoliter Continuous Reactor, ACS
751 Appl. Mater. Interfaces. 5 (2013) 9405–9410. doi:10.1021/am4029872.

752 [47] Y.J. Hwang, C.W. Coley, M. Abolhasani, A.L. Marzinzik, G. Koch, C. Spanka, H.
753 Lehmann, K.F. Jensen, A segmented flow platform for on-demand medicinal chemistry
754 and compound synthesis in oscillating droplets, Chem. Commun. 53 (2017) 6649–6652.
755 doi:10.1039/c7cc03584e.

756 [48] M. Faustini, J.J.Y. Kim, G. Jeong, J.J.Y. Kim, H.R. Moon, W. Ahn, D. Kim, Microfluidic
757 Approach toward Continuous and Ultrafast Synthesis of Metal–Organic Framework
758 Crystals and Hetero Structures in Confined Microdroplets, J. Am. Chem. Soc. 135 (2013)
759 14619–14626. doi:10.1021/ja4039642.

760 [49] D.M. Holunga, R.C. Flagan, H.A. Atwater, A Scalable Turbulent Mixing Aerosol Reactor
761 for Oxide-Coated Silicon Nanoparticles, Ind. Eng. Chem. Res. 44 (2005) 6332–6341.
762 doi:10.1021/ie049172l.

763 [50] A. Parulkar, N.A. Brunelli, High-Yield Synthesis of ZIF-8 Nanoparticles Using
764 Stoichiometric Reactants in a Jet-Mixing Reactor, Ind. Eng. Chem. Res. 56 (2017) 10384–

765 10392. doi:10.1021/acs.iecr.7b02849.

766 [51] A. V. Nikam, A.A. Kulkarni, B.L.V. Prasad, Microwave-assisted batch and continuous
767 flow synthesis of palladium supported on magnetic nickel nanocrystals and their
768 evaluation as reusable catalyst, Cryst. Growth Des. 17 (2017) 5163–5169.
769 doi:10.1021/acs.cgd.7b00639.

770 [52] K.W. Brinkley, The Synthesis of Solid Supported Palladium Nanoparticles : Effective
771 Catalysts for Batch and Continuous Cross Coupling Reactions, Virginia Commonwealth
772 University, 2015.

773 [53] S. Cattaneo, S. Althahban, S.J. Freakley, M. Sankar, T. Davies, Q. He, N. Dimitratos, C.J.
774 Kiely, G.J. Hutchings, Synthesis of highly uniform and composition-controlled gold-
775 palladium supported nanoparticles in continuous flow, Nanoscale. 11 (2019) 8247–8259.
776 doi:10.1039/c8nr09917k.

777 [54] C.A. Schneider, W.S. Rasband, K.W. Eliceiri, NIH Image to ImageJ: 25 years of image
778 analysis, Nat. Methods. 9 (2012) 671–675. doi:10.1038/nmeth.2089.

779 [55] E.A. Barringer, H.K. Bowen, Formation, Packing, and Sintering of Monodisperse TiO2
780 Powders, J. Am. Ceram. Soc. 65 (1982) C-199-C-201. doi:10.1111/j.1151-
781 2916.1982.tb09948.x.

782 [56] M.T. Harris, C.H. Byers, Effect of solvent on the homogeneous precipitation of titania by
783 titanium ethoxide hydrolysis, J. Non. Cryst. Solids. 103 (1988) 49–64. doi:10.1016/0022-
784 3093(88)90415-2.

785 [57] N.Y. Turova, E.P. Turevskaya, V.G. Kessler, M.I. Yanovskaya, eds., The Chemistry of

786 Metal Alkoxides, Springer US, 2002. doi:10.1007/b113856.

787 [58] Z. Yang, K.J. Klabunde, Synthesis of nearly monodisperse palladium (Pd) nanoparticles
788 by using oleylamine and trioctylphosphine mixed ligands, J. Organomet. Chem. 694
789 (2009) 1016–1021. doi:10.1016/j.jorganchem.2008.11.030.

790 [59] C.H. Lien, J.W. Medlin, Promotion of activity and selectivity by alkanethiol monolayers
791 for Pd-catalyzed benzyl alcohol hydrodeoxygenation, J. Phys. Chem. C. 118 (2014)
792 23783–23789. doi:10.1021/jp507114g.

793